SANDIA REPORT

SAND2012-6527
Unlimited Release
Printed August 2012

On the Nonlinear Dynamics and Quasi-Statics of Tape Joined Structures

Daniel J. Segalman and Michael J. Starr

Prepared by
Sandia National Laboratories
Albuquerque, New Mexico 87185 and Livermore, California 94550

Sandia National Laboratories is a multi-program laboratory managed and operated by Sandia Corporation, a wholly owned subsidiary of Lockheed Martin Corporation, for the U.S. Department of Energy's National Nuclear Security Administration under contract DE-AC04-94AL85000.

Approved for public release; further dissemination unlimited.

Sandia National Laboratories

Issued by Sandia National Laboratories, operated for the United States Department of Energy by Sandia Corporation.

NOTICE: This report was prepared as an account of work sponsored by an agency of the United States Government. Neither the United States Government, nor any agency thereof, nor any of their employees, nor any of their contractors, subcontractors, or their employees, make any warranty, express or implied, or assume any legal liability or responsibility for the accuracy, completeness, or usefulness of any information, apparatus, product, or process disclosed, or represent that its use would not infringe privately owned rights. Reference herein to any specific commercial product, process, or service by trade name, trademark, manufacturer, or otherwise, does not necessarily constitute or imply its endorsement, recommendation, or favoring by the United States Government, any agency thereof, or any of their contractors or subcontractors. The views and opinions expressed herein do not necessarily state or reflect those of the United States Government, any agency thereof, or any of their contractors.

Printed in the United States of America. This report has been reproduced directly from the best available copy.

Available to DOE and DOE contractors from
U.S. Department of Energy
Office of Scientific and Technical Information
P.O. Box 62
Oak Ridge, TN 37831

Telephone: (865) 576-8401
Facsimile: (865) 576-5728
E-Mail: reports@adonis.osti.gov
Online ordering: http://www.osti.gov/bridge

Available to the public from
U.S. Department of Commerce
National Technical Information Service
5285 Port Royal Rd
Springfield, VA 22161

Telephone: (800) 553-6847
Facsimile: (703) 605-6900
E-Mail: orders@ntis.fedworld.gov
Online ordering: http://www.ntis.gov/help/ordermethods.asp?loc=7-4-0#online

SAND2012-6527
Unlimited Release
Printed August 2012

On the Nonlinear Dynamics and Quasi-Statics of Tape Joined Structures

Daniel J. Segalman
Multi-Physics Modeling & Simulation Department
djsegal@sandia.gov

Michael J. Starr
Component Science & Mechanics
mjstarr@sandia.gov

Sandia National Laboratories
PO Box 969, Mail Stop 9042
Livermore, CA 94551-0969

Abstract

Tape joints have been a key tool in assembly of nuclear weapons for almost 40 years. In that time sufficient experience has been gained to have confidence on the robustness of this technology within established design constraints; the structural dynamics of systems assembled by tape joints are much less well understood. Though there is lore that tape joined structures behave linearly in the axial direction, even that is contradicted by the literature, where such structures are found to be bi-linear (nonlinear) in axial modes. Experimental results presented here show much more significant nonlinearity when such systems vibrate in such a way that there is bending across the joint cross-section.

In addition, it will be difficult to understand the nonlinear structural dynamics before the pre-loads on the tape joints is known. Therefore, a strategy to deduce the joint pre-loads from surface strain measurements has been developed. This technique exploits finite element analysis to generate an approximate Green's function to map tape loads to surface strain and employs numerical optimization to solve an inverse problem. This technique is demonstrated on the same test specimen employed in the dynamics experiments.

Acknowledgment

The authors thank Chi S. (”David”) Lo and Jeff Payne for their continued support and patience with respect to the analytic portion of this work. Laura Jacobs-O’Malley is thanked for funding the experimental portion of this work.

Michael Jew designed the test specimen employed in this study, but was drawn off by other urgencies before he could perform the tests. That work fell into the hands of Everest Sewell who took the data, Todd Simmermacher who supervised, and Brandon Zwink who helped translate it to Matlab readable form.

The authors especially appreciate some very useful suggestions made by Randall Mayes and Michael Ross with respect to the preparation of this report.

Contents

1 Introduction **9**

2 Nonlinear Vibration of a Tape-Joined Structure **11**

3 Contact Nonlinearity and Vibration **15**

4 Geometry and Assembly of Tape Joints **19**

5 Quasi-Static Analysis **23**
Tape Joint Equilibrium 23
Elasticity, Symmetry, and Inverse Problems 24
The Forward Problem 24
The Inverse Problem 25
Solving the Inverse Problem 26
An Exploitation of Axial Symmetry 28

6 The Quasi-Static Experiment **29**
Test Specimen 29
Strain Gauges 29
The Test 30

7 Finite Element Analysis **39**

8 Results **41**
Assembly 1 41
Assembly 2 43
Future Cautions 45

9 Conclusion **47**

References **48**

Appendix

A The Softening Duffing Oscillator **51**

B A Reduced Tape-Joint Model for Finite Element Analysis **53**

List of Figures

2.1 *The assembled tape joint test specimen is shown on the left. The locations of the accelerometers is shown on the right, each semi-circular band indicating the axial location of three tri-axial accelerometers. The accelerometers at the end of solid lines are visible to the camera and the accelerometers at the end of dashed lines are on the opposite side.* 11

2.2 *The frequency response of a point at the center of the test specimen to steady state sinusoidal excitation on the rim. The force amplitudes are 1 lb (blue) , 5 lb (green), 10 lb (red). Solid lines are associated with tests employing downward sweeps in excitation frequency and dashed lines are associated with upward sweeps in excitation frequency.* 12

3.1 *At low amplitudes of vibration , the "point of closure" remains closed and the system behaves as though that surface were welded (upper figure). At much higher vibration amplitudes, the "surface of closure" may open at some locations along its circumference (lower figure).* 15

3.2 *An illustration of a system for which tangent stiffness changes instantaneously as a pre-load is overcome by system dynamics.* 16

3.3 *The nonlinearity of the system shown in Figure 3.2 is presented here via the dependence of resonance frequency on excitation amplitude.* 18

4.1 *In this figure of Alvis [1], the tape joint is treated as version of Tongue-and-Groove joint.* 19

4.2 *The various elements of the standard tape joint are indicated in this figure of Rechard et al. [2].* 20

4.3 *Opposing wedges are placed in the tape joint slot so that converging motion of those "tapes" pushes against the sides of the slot and locks the joint. (This figure from [2]).* 20

4.4 *Tape joints are usually used to connect cylinders in an end-to-end manner (This figure from [3]).* 21

4.5 *Insertion of the tapes is done through windows in the wall of the outer (female) cylinder. (This figure from [2]).* 22

4.6 *The tapes are manufactured with regular slots so that they will bend easily about the axis of the cylinders. (This figure from [2]).* 22

5.1 *At each place along its track, the tape joint applies equal and opposite loads on each of the two constituent units.* 23

5.2 *Segment k on which basis force F_k is applied.* 25

6.1 *The insertion window as seen in the assembled system and in the female component alone.* . . . 29
6.2 *The tapes in their original state and as they appear after having been used in a tape joint assembly and then removed.* . . . 30
6.3 *The various steps in the testing process are reflected in the axial strain histories. These strains are from Assembly 1.* . . . 31
6.4 *Axial strains on the male and female components at* 90° *and* 270° *on Assembly 1.* . . 33
6.5 *Hoop strains from Assembly 1.* . . . 34
6.6 *Axial strain histories from Assembly 2.* . . . 35
6.7 *Axial strains on the male and female components at* 90° *and* 270°. . . . 36
6.8 *Hoop strains from Assembly 2.* . . . 37

7.1 *Finite element mesh in vicinity of tape joint.* . . . 39
7.2 *Circumferential distribution of surface strains on the male component due to a concentrated force at* 0°. . . . 40
7.3 *Circumferential distribution of surface strains on the female component due to a concentrated force at* 0°. . . . 40

8.1 *Circumferential distribution of tape load computed for Assembly 1.* . . . 41
8.2 *Circumferential distribution of axial strain for Assembly 1 from measurement and from computed tape load.* . . . 42
8.3 *Circumferential distribution of hoop strain for Assembly 1 from measurement and from computed tape load.* . . . 42
8.4 *Circumferential distribution of tape load computed for Assembly 2.* . . . 43
8.5 *Circumferential distribution of axial strain for Assembly 2 from measurement and from computed tape load.* . . . 44
8.6 *Circumferential distribution of hoop strain for Assembly 2 from measurement and from computed tape load.* . . . 44

A.1 *The softening Duffing oscillator admits multiple response amplitudes at fixed amplitude of harmonic excitation. "Up-jumps" and "down-jumps" in amplitude occur at the driving frequency is swept up or down, respectively.* . . . 52

B.1 *The assembled system is modeled as two physical components jointed by a zero-thickness interface whose properties are to be found.* . . . 53
B.2 *The joint is modeled as a finitely deformable, but infinitesimally thick material.* . . 54

List of Tables

2.1 Resonant amplitudes and frequencies associated with three levels of excitation. . . 13

6.1 Angular locations of strain gauges 30

Chapter 1

Introduction

Tape joints have been part of the assembly of nuclear weapons for almost forty years. The original patent was submitted by a Sandian, Robert L. Alvis, in 1969 [4]. The appeal of tape joints for this purpose was enumerated early on by Huerta and Black [3]; tape joints are

1. Strong,
2. Lightweight,
3. Easily assembled, and
4. Provide a smooth exterior surface

It is also desirable that the joint not consume a large amount of internal volume. In some instances it must be assembled without access to the interior [3]. With respect to the above criteria, the tape joint is an excellent method of attachment.

There is another category of requirements that were not explicitly discussed in [3], but were recognized in later publications: the necessity of predicting joint response mathematically as part of the design process. To this end, Rechard et al. [2] addressed the calculation of joint strength and later Rechard performed finite element analysis to interpret axial stiffness of tape-joined structures [5].

With increasing reliance on the results of computer simulation to make design and certification decisions, predictive capability with respect to other aspects of tape joints is increasingly important. One such area requiring better predictive capability is that of the dynamics and vibrations of tape joined structures.

The quasistatic experiments investigated by Rechard found that the axial stiffness of jointed structures was bi-linear (nonlinear), substantially stiffer in compression than in tension. More recent dynamic (vibration) data of such structures in bending, presented in the first portion of this report, demonstrate them to be highly nonlinear, with frequency decreasing with vibration amplitude. These nonlinearities, and others, appear to derive from linear elastic contact mechanics in the vicinity of the joints. Understanding, quantifying, and predicting that mechanics requires understanding the pre-load in the structure due to the tapes.

Because all of the action is taking place on interfaces inaccessible to the experimentalist, assessing that preload must be done indirectly. How one can do this via surface mounted strain gauges, finite element approximations for a Green's function, and the solution of a mathematical inverse problem is presented in the second portion of this report.

Chapter 2

Nonlinear Vibration of a Tape-Joined Structure

A test specimen consisting of two cylindrical aluminum components and the machined features necessary for tape (stainless steel) assembly was constructed to explore both the dynamic and quasistatic behavior. The assembled system is shown on the left hand side of Figure 2.1. In this experiment and in the experiments discussed in a later chapter, the female component is suspended from above by a soft spring and the male component is attached by a tape joint and hangs below. In the dynamic experiments, a shaker imposed harmonic excitations at fixed force amplitude at the lower rim of the male component. Tri-axial accelerometers were placed as indicated in the right hand side of Figure 2.1. These experiments involved upward sweeps in frequency and then corresponding downward sweeps in frequency.

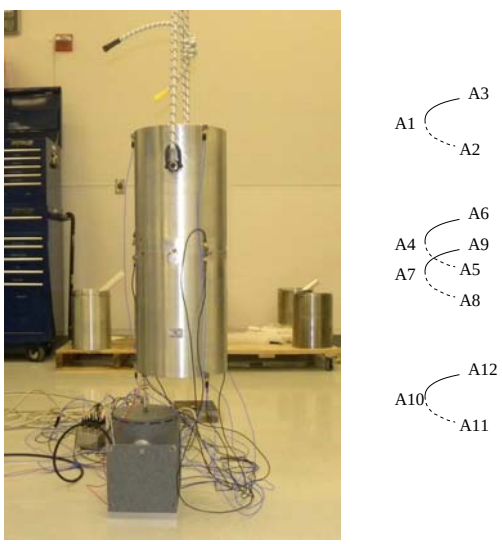

Figure 2.1: *The assembled tape joint test specimen is shown on the left. The locations of the accelerometers is shown on the right, each semi-circular band indicating the axial location of three tri-axial accelerometers. The accelerometers at the end of solid lines are visible to the camera and the accelerometers at the end of dashed lines are on the opposite side.*

These dynamic experiments yielded apparent frequency response functions (FRF) near the joint (location 4 of the figure) due to excitation at the rim (location 10 of the figure). These are shown

in Figure 2.2.

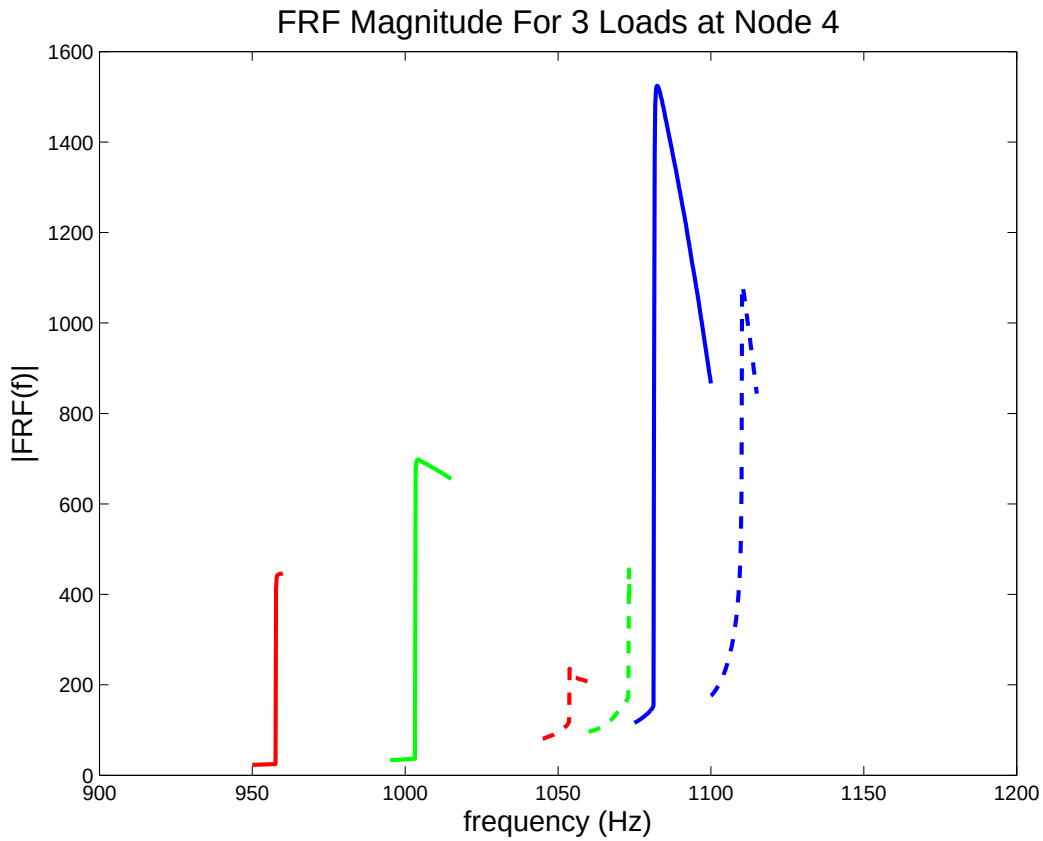

Figure 2.2: *The frequency response of a point at the center of the test specimen to steady state sinusoidal excitation on the rim. The force amplitudes are 1 lb (blue) , 5 lb (green), 10 lb (red). Solid lines are associated with tests employing downward sweeps in excitation frequency and dashed lines are associated with upward sweeps in excitation frequency.*

The different colors correspond to different levels of excitation amplitude: amplitudes are 1 lb (blue) , 5 lb (green), 10 lb (red). The dashed lines are the frequency responses measured from up-sweeps in frequency at fixed amplitude and the solid lines are the corresponding frequency response functions as the frequency is swept down.

Were this a linear structure, all six frequency response plots associated would overlie each other. Figure 2.2 dramatically shows the nonlinearity of this test specimen. Three more observations are to be made from this figure:

1. The amplitude of the FRFs can vary by as much as a factor of three with amplitude. Not only is this a strong proof of nonlinearity, it is a strong argument that nonlinearity cannot be ignored in structural dynamics of tape-joined systems.

2. The peak acceleration associated with upward frequency sweeps is lower than that associated with downward frequency sweeps at the same excitation frequency.

3. For fixed excitation amplitude, that downward sweeping of excitation frequency yields apparent resonance at a lower frequency than does upward sweeping of excitation frequency at the same amplitude. This is an indication of systems that soften with amplitude [6].

4. The up-slope of the FRF curves is much steeper than the down slope. This is also a feature of a softening response [7].

The frequencies and amplitudes of the FRF peaks are shown quantitatively in Table 2.1.

Table 2.1: Resonant amplitudes and frequencies associated with three levels of excitation.

Frequency Sweep	Excitation Amp. (lb)	Resonance Peak (Hz)	FRF Amp. Node 4
down	1	1082	1524
down	5	1004	698
down	10	959	446
up	1	1110	1083
up	5	1073	455
up	10	1054	236

Observations 2, 3 and 4 might be made understandable by consideration of a softening Duffing oscillator, discussed in Appendix A. Such oscillators are characterized by stiffnesses that decrease strongly with displacement amplitude and have resulting nonlinear dynamic properties, including the three spelled out above. This is not to argue that tape-joined structures are Duffing oscillators, but rather to note that dynamic properties of the test structure are sufficiently similar to those of Duffing oscillators to infer that the underlying cause is a strong nonlinear softening.

Given the extraordinary dynamic nonlinearity of tape-joined structures suggested by these experiments, it is incumbent on the analyst to accommodate these nonlinearities in any meaningful structural dynamics simulation. This requires some qualitative understanding of the nonlinear mechanics at the root of this dynamic behavior, some meaningful way of representing this nonlinearity in structural dynamics simulations, and physically meaningful approaches to parameterizing such models.

The first step is to develop techniques to interpret experimental data to understand something of the load state inside the joint. The rest of the body of this report is devoted to such an initiative.

Chapter 3

Contact Nonlinearity and Vibration

The qualitative explanation for the above nonlinearity is as follows:

1. At low amplitudes of vibration, the "point of closure" remains closed and the system behaves as though that surface were welded [5]. (A discussion of tape joint geometry is presented in the next chapter.)

2. On the other hand, at high amplitudes of vibration (as suggested in Figure 3.1), the inertial loads may cause deformations that overcome the preloads. As the contact patch is opened, the effective stiffness of the system decreases.

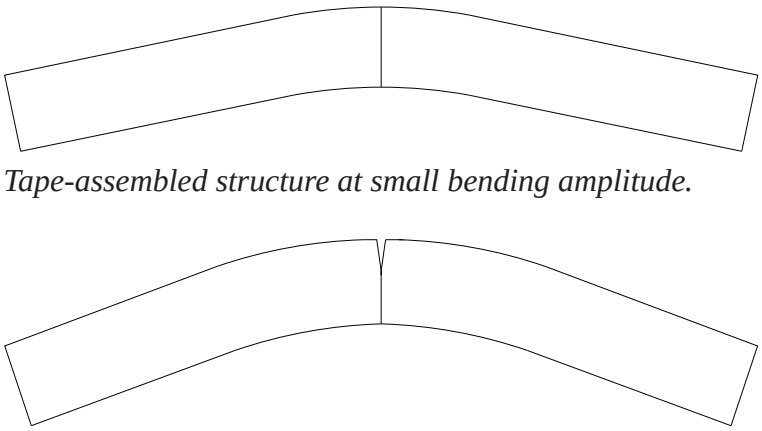

Tape-assembled structure at small bending amplitude.

Tape-assembled structure at large bending amplitude.

Figure 3.1: *At low amplitudes of vibration , the "point of closure" remains closed and the system behaves as though that surface were welded (upper figure). At much higher vibration amplitudes, the "surface of closure" may open at some locations along its circumference (lower figure).*

This explanation is consistent with axial experiments reported by Rechard [5] and his accompanying two dimensional finite element analyses. In the reported experiments, the jointed structure appeared to behave as a stiff linear system in tension and as a much stiffer linear system in compression. The finite element analyses gave qualitatively similar results, but the load at which response switched from one linear system to another could not be calculated because the tape load was unknown. It should be emphasized that the mechanisms elicited in quasistatic axial experiments and

calculations reported by Rechard are in some ways qualitatively different from bending mechanisms - most importantly, in bending the load increases on some portion of the point-of-closure while it decreases at points on the opposite side of the neutral axis.

The more classical studies involved single degree of freedom systems with the contact nonlinearity represented as a nonlinear spring. Examples include those where the nonlinear stiffness is approximated as a Hertzian contact [8, 9, 10]. In these problems, normal stiffness goes as preload to the 3/2 power, so the contact is stiffer than the reference state in one part of the cycle and softer than the reference state in another part of the cycle.

More representative of the tape joint system is that shown in Figure 3.2. Here the reference state is that where the massless platform A, is pinned to the foundation by a pre-load P_0 and massless platform B is similarly pinned to an opposite foundation.

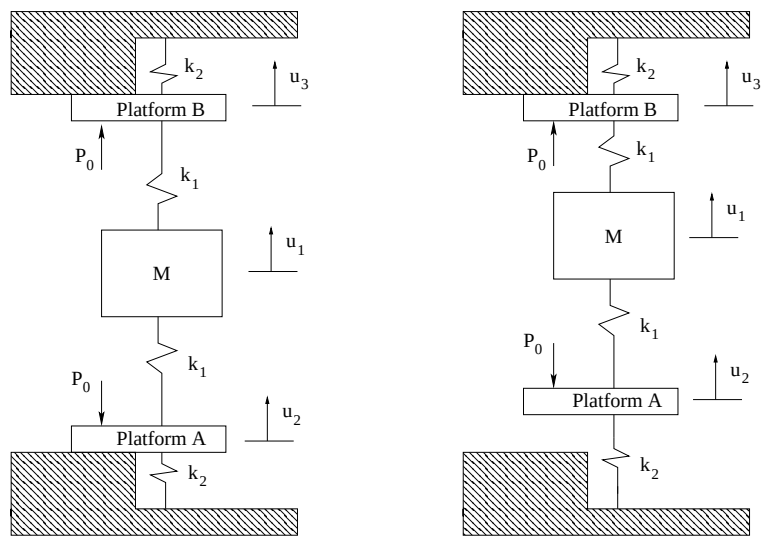

Figure 3.2: *An illustration of a system for which tangent stiffness changes instantaneously as a pre-load is overcome by system dynamics.*

In the reference state, the stiffness of the single degree of freedom system involving mass M is $2k_1$, the governing equation is

$$M\ddot{u}_1 + 2k_1 u_1 = 0 \tag{3.1}$$

and the natural frequency is $\omega_0 = \sqrt{2k_1/M}$. Once the dynamic loads are such that $k_1 u_1 > P_0$, platform A lifts off the foundation and the governing equation for the motion of mass M suddenly changes to

$$M\ddot{u}_1 + k_1\left(\frac{k_1 + 2k_2}{k_1 + k_2}\right)u_1 = -P_0\frac{k_1}{k_1 + k_2} \tag{3.2}$$

and the natural frequency in this portion of the cycle is $\omega_1 = \omega_0\sqrt{\frac{(k_1+2k_2)}{2(k_1+k_2)}} < \omega_0$. Similarly when $-k_1u_1 > P_0$, platform B lifts off its foundation, The governing equation becomes:

$$M\ddot{u}_1 + k_1\left(\frac{k_1+2k_2}{k_1+k_2}\right)u_1 = P_0\,\frac{k_1}{k_1+k_2} \tag{3.3}$$

and the natural frequency again drops to $\omega_1 = \omega_0\sqrt{\frac{(k_1+2k_2)}{2(k_1+k_2)}} < \omega_0$.

In this system the stiffness changes discontinuously over the cycle. This transition from one linear system to another is actually a nonlinear feature.

1. This is seen in the time domain by consideration of two identical acceleration signals applied to the structure. Say each of these is 90% of that necessary to lift Platform A from its base. Each of them separately elicits the response of a simple harmonic oscillator of frequency ω_0. Applied together, they elicit a much more complex response, including a switching of governing equation in the middle of each cycle. Superposition is violated.

2. This is seen in the frequency domain by a comparison of responses to different amplitude pulses. For small excitation, the response is exclusively at frequency ω_0, but for much larger excitation levels, the response frequency (in a harmonic balance sense) drops. This is again a violation of linearity.

This last feature is illustrated for the system of Figure 3.2 in Figure 3.3. For this case, $k_1 = 1$, $k_2 = 1/2$, $M = 1$, and $P_0 = 1$, the natural frequency shows a strong dependence on vibration amplitude. At very small amplitude, the natural frequency is near its exact value, $\sqrt{2}$ and frequency stays steadily there until amplitude exceeds the value of 1. Beyond that point the frequency decreases monotonically. (Each point in this graph represents the solution of the dynamic system over a full cycle. Periodicity is enforced by requiring that each state variable have the same value at the end of the cycle as it had at the beginning.)

This behavior is qualitatively similar to that found experimentally with our tape-assembled test structure. This similarity argues that the nonlinearity of the tape joint vibrations is also due to a process of gaps opening and closing. If that is the case, just as is the case in the simple mechanism explored here, knowledge of preload (in this case tape loads) is a prerequisite to development of quantitatively correct dynamics models.

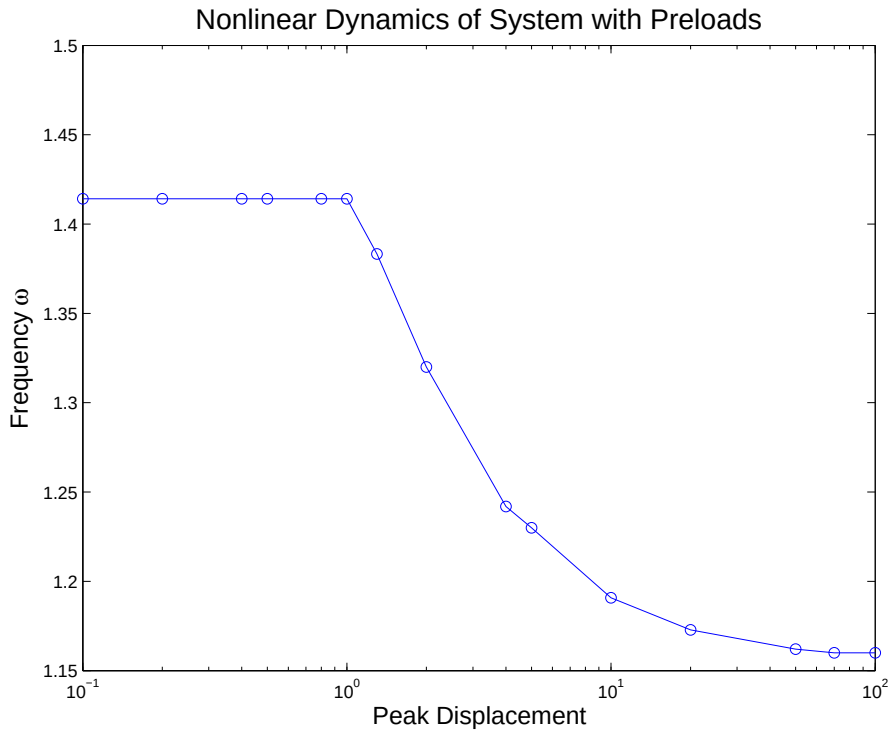

Figure 3.3: *The nonlinearity of the system shown in Figure 3.2 is presented here via the dependence of resonance frequency on excitation amplitude.*

Chapter 4

Geometry and Assembly of Tape Joints

Alvis [1] explains tape joints as a species of tongue-and-groove joint (see Figure 4.1.) The first enhancement on the standard tongue-and-groove (TG) joint is the use of two displaced TG joints to restrict relative rotation. Further the TG joints are held closed by a slot into which an expanding insert is placed.

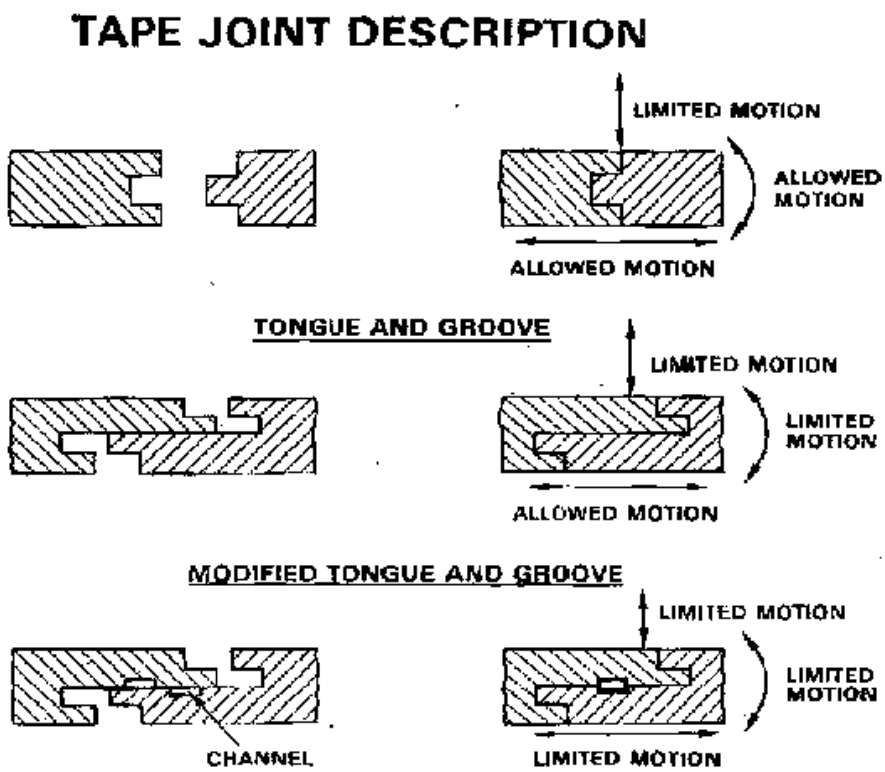

Figure 4.1: *In this figure of Alvis [1], the tape joint is treated as version of Tongue-and-Groove joint.*

The various elements of a standard tape joint are show in Figure 4.2. Of particular note are the locking slot, indicated by annotation “Tape Segments”, and contact location indicate by the annotation “Point of Closure”.

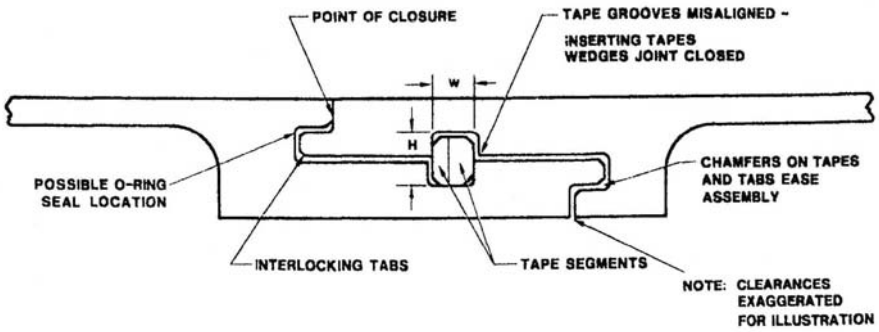

Figure 4.2: *The various elements of the standard tape joint are indicated in this figure of Rechard et al. [2].*

The tape is designed so that if two halves of the slot were aligned, there would be a large compressive force a the point of closure. How the insert moves the two sides of the slots toward alignment and causes compression at the point of closure is indicated in Figure 4.3

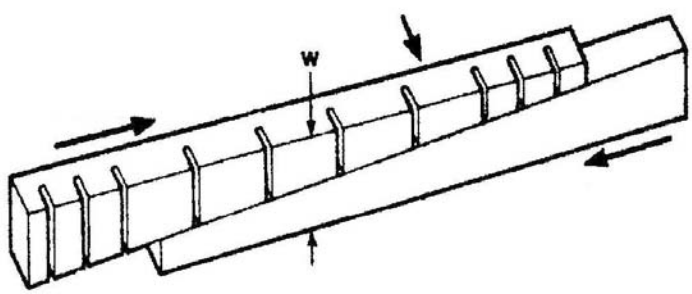

Figure 4.3: *Opposing wedges are placed in the tape joint slot so that converging motion of those “tapes” pushes against the sides of the slot and locks the joint. (This figure from [2]).*

Tape joints are usually used to attach cylinders end to end in the manner shown in Figure 4.4. (A very different sort of tape joint is investigated in [11].)

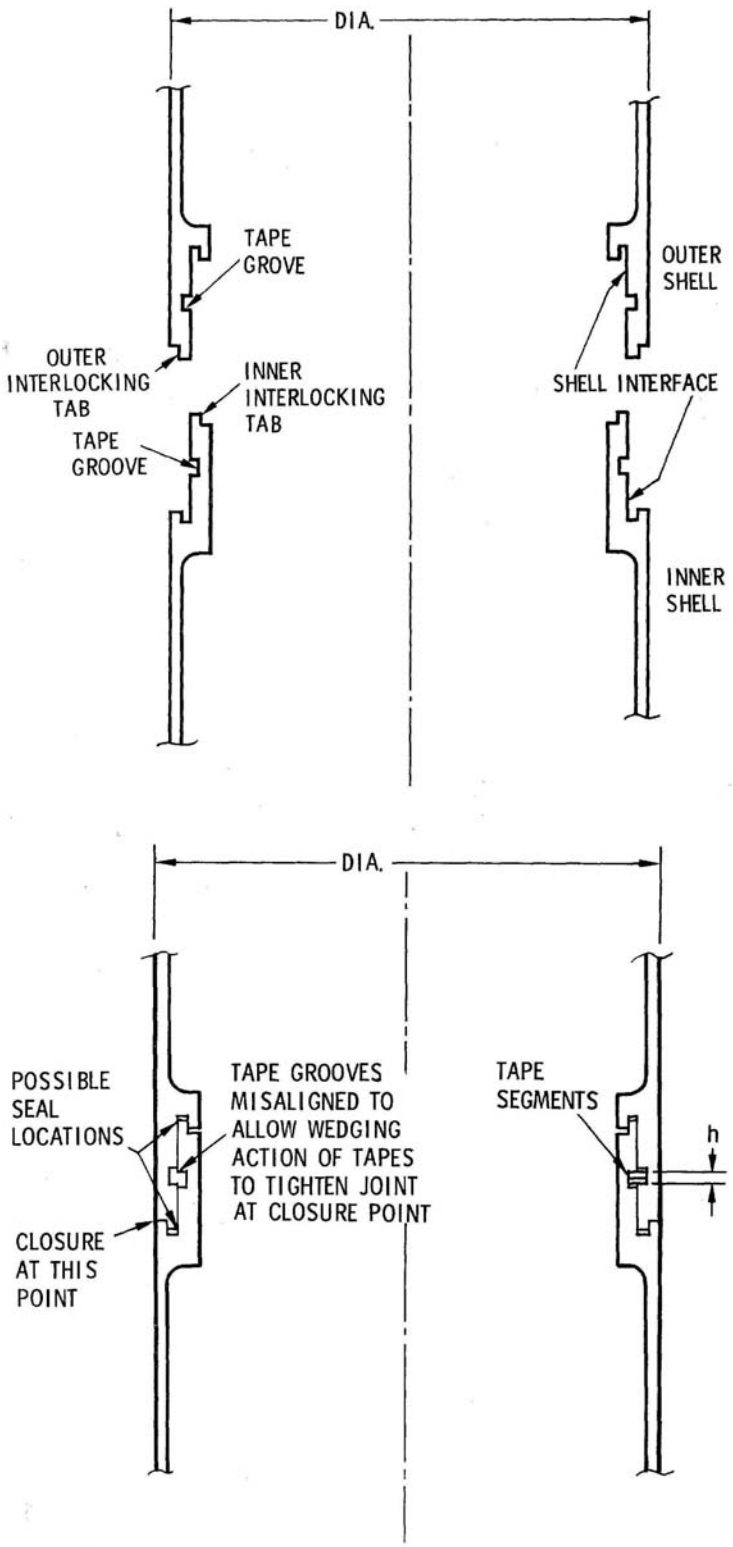

Figure 4.4: *Tape joints are usually used to connect cylinders in an end-to-end manner (This figure from [3]).*

Insertion of the tapes is done through at least two windows in the walls of the outer cylinder. (See Figure 4.5). In fact, the nomenclature is clarified by observing that it is the female component that has the windows through which the tapered wedges are placed.

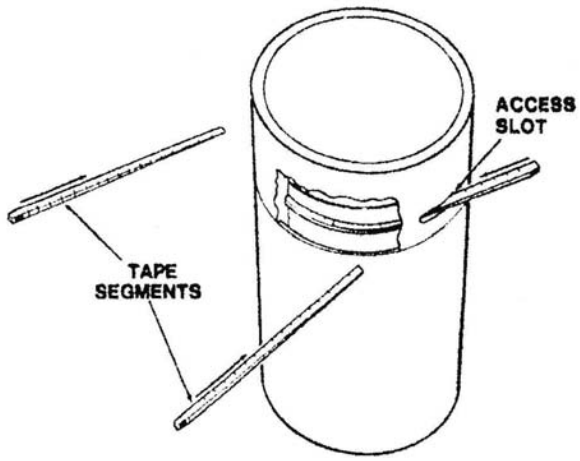

Figure 4.5: *Insertion of the tapes is done through windows in the wall of the outer (female) cylinder. (This figure from [2]).*

The tapes are manufactured with regular slots so that they will bend easily about the axis of the cylinders. This is illustrated in Figure 4.6.

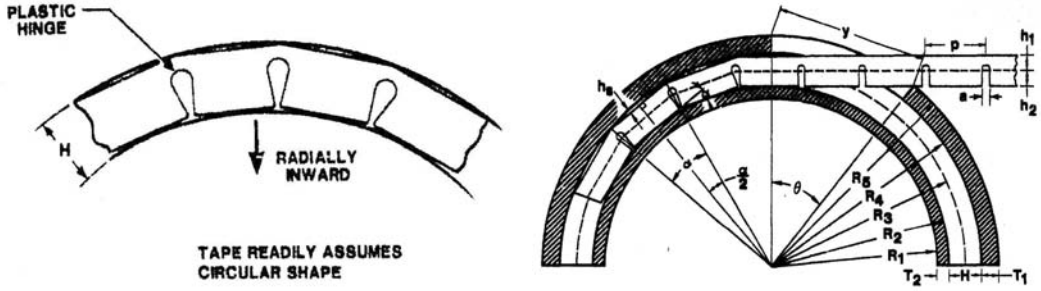

Figure 4.6: *The tapes are manufactured with regular slots so that they will bend easily about the axis of the cylinders. (This figure from [2]).*

Chapter 5

Quasi-Static Analysis

Tape Joint Equilibrium

Consider a structure consisting of two subsystems connected by a tape joint. Each subsystem is considered to be linear, so the only nonlinearity is that associated with their connection.

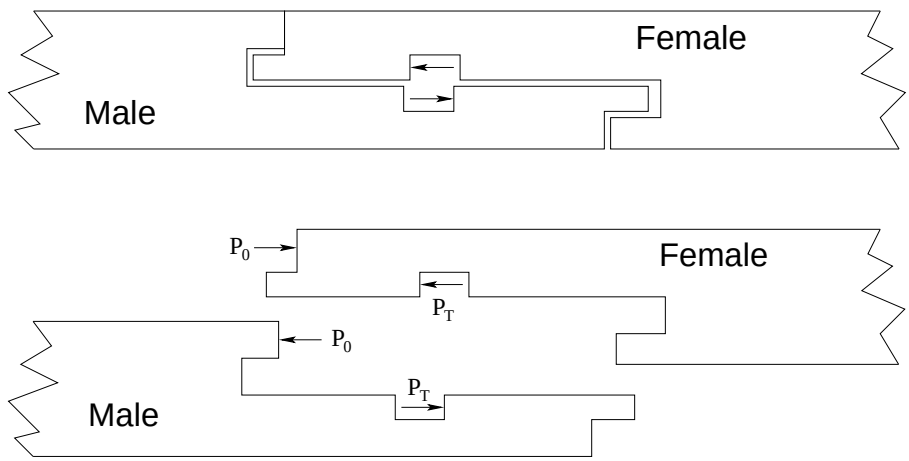

Figure 5.1: *At each place along its track, the tape joint applies equal and opposite loads on each of the two constituent units.*

Consider the system whose cross-section is shown in Figure 5.1. At each point along the tape track the tape applies roughly equal and opposite loads to the male and female components. These are marked as $P_T(\theta)$ where θ is the circumferential angle identifying the cross section. The units of P_T are force/unit length. Each of the bodies is held in equilibrium by forces $P_0(\theta)$ at the "point of closure" (see Figure 4.2.).

The tape forces and the closure forces do not have quite the same values.

1. The contribution to net force on each body at each arc $d\theta$ from tape force is $P_T(\theta)r_T d\theta$ where r_T is the radius of the tape channel. The contribution of the closure force is $P_0(\theta)r_0 d\theta$. So the two forces are related on average by the ratio r_0/r_T.

2. The tape force $P_T(\theta)$ is expected to vary substantially with θ. Because the point of closure is a significant distance from the tape, the closure force there will be influenced in an integrated sense by values of P_T in a neighborhood of cross-sections including θ.

It is the tape loads, $P_T(\theta)$, acting through the elasticity of the bodies that are responsible for the pre-loads at the point-of-closure. The most fundamental challenge to predictive dynamics modeling of tape-assembled structures is deducing these tape loads.

Elasticity, Symmetry, and Inverse Problems

Tape forces cannot be directly measured; for an array of force transducers cannot be put inside the joint or along the annulus. However, strains on the external surface of the structure can be measured. (With a bit more difficulty, surface strains could also be measured inside the interior of the structure.) The remainder of this section discusses using that experimental data to deduce tape loads.

The Forward Problem

Consider the forward problem: if the load distribution $P_T(\theta)$ on the tape is known, then the surface strains on the structure can be calculated with the enforcement of some simplifications. The first step is to re-pose the problem to be linear. This is done by removing all contact uncertainties:

1. The "point of closure" is treated as welded. This assumption worked fairly well for Rechard [5] when modeling the assembled system under compression.

2. The tape is replaced with a distribution of equal and oppositely applied forces $F_T(\theta)$ along the tape joint track, as suggested in Figure 5.1. It is these forces that are desired.

Consistent with assumption 2 above, the following discretization for the tape force is introduced. Divide the surface of the tape track into annular segments so that the kth segment is centered at angle θ_k, having angular width, $d\theta_k$, and having radial depth dr equal to the radial projection of the tape onto its track. (See Figure 5.2.) On angular segment k, a uniform pressure p_k numerically equal to F_k/r is applied. This corresponds numerically to F_k units force per unit circumferential length.

Numerically, the forward question is:

> given a vector $\mathscr{F}_T$ of discretized forces $\{F_k\}$ applied along the tape track, calculate the displacements and strains at selected locations on and within the structure.

In a displacement-based finite element formulation this is achieved in two steps:

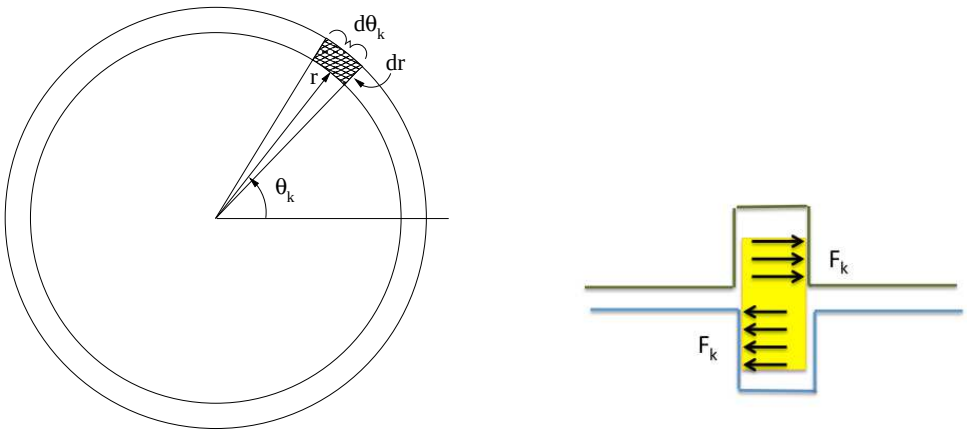

Figure 5.2: *Segment k on which basis force F_k is applied.*

1. Given the applied force vector $\mathscr{F}$, the displacement field $\mathscr{U}$ is found from

$$K\mathscr{U} = \mathscr{F}_T \tag{5.1}$$

   where stiffness matrix K could be expected to be well conditioned.

2. The strain field can be deduced from the displacements

$$\varepsilon_j = B_j \mathscr{U} \tag{5.2}$$

where ε_j refers to the strain at location j on the surface of the structure. Solution of Eq. (5.1) for $\mathscr{U}$ given $\mathscr{F}_T$ is the forward problem.

The Inverse Problem

The inverse problem involves estimating the (unobservable) tape loads. Elements of the direct solution are used to pose the inverse problem mathematically.

For each segment number k, define the basis force vector $\mathscr{F}_{T,k}$ such that it is zero in all rows but the kth and has the value of one on the kth row.

The vector of tape forces can be constructed using these basis vectors:

$$\mathscr{F}_T = \sum_k \mathscr{F}_{T,k} F_k \tag{5.3}$$

Equation (5.1) can be solved for the displacement field corresponding to basis force $\mathscr{F}_{T,k}$:

$$K\mathscr{U}_k = \mathscr{F}_{T,k} \tag{5.4}$$

which must be solved for each k.

From $\mathscr{U}_k$ the contribution of $\mathscr{F}_{T,k}$ to the jth strain is found from

$$\varepsilon_{j,k} = B_j \mathscr{U}_k \tag{5.5}$$

Because of linearity,

$$\varepsilon_j = \sum \varepsilon_{j,k} F_k \tag{5.6}$$

In matrix form, this is

$$\varepsilon = H \mathscr{F}_T \tag{5.7}$$

The inverse problem consists of employing Eq. (5.7) and some measured surface strains to deduce $\mathscr{F}_T$.

Solving the Inverse Problem

In general, the inverse problem is ill-posed. It is ill-posed not only because the number of equations usually differs from the number of unknowns, but also because a multitude of combinations of unknown forces could generate the known strains almost equally well.

In this problem, the ill-posedness is addressed in three steps.

1. The problem of Eq. (5.7) is converted to the following optimization problem:

$$\text{Minimize} \quad J_0(\mathscr{F}_T) = (H\mathscr{F}_T - \varepsilon)^T (H\mathscr{F}_T - \varepsilon) \tag{5.8}$$

   This addresses issues of minor inconsistencies in data and it makes it possible to address issues of the rank of H via the following steps.

2. For physical reasons, it is expected that the tape applies only compressive tractions to the surfaces of its channel. Therefore the optimization is restricted to forces satisfying

$$F_k \leq 0 \tag{5.9}$$

   for all k.

3. There remains a non-uniqueness problem. There are still many combinations of force vector $\mathscr{F}_T$ that satisfy the above inequality and minimize J_0 equally well; the optimization remains ill-posed. This is addressed with the use of Tikhonov regularization [12]. The objective function is changed as follows:

$$\text{Minimize} \quad J_1(\mathscr{F}_T) \tag{5.10}$$

where

$$J_1(\mathscr{F}_T) = J_0(\mathscr{F}_T) + \alpha_1 \mathscr{F}_T^T I_N \mathscr{F}_T + \alpha_2 \mathscr{F}_T^T S^T S \mathscr{F}_T + \alpha_3 \sum_i \mathscr{F}_T^T \hat{H}_i^T S^T S \hat{H}_i \mathscr{F}_T \tag{5.11}$$

Above,

- Matrix I_N is the identity matrix whose dimension is that of $\mathscr{F}_T$. This term is necessary to assure that the components of the solution vector are bounded.
- Matrix S captures the second central difference of the array it multiplies. The product of it and any vector is roughly the curvature of that vector as measured circumferentially

$$S = \begin{bmatrix} 2 & -1 & 0 & \cdots & & -1 \\ -1 & 2 & -1 & \cdots & & 0 \\ 0 & -1 & 2 & -1 & \cdots & 0 \\ \vdots & \vdots & \vdots & \vdots & \vdots & \vdots \\ -1 & \cdots & \cdots & \cdots & -1 & 2 \end{bmatrix} \tag{5.12}$$

  The -1 on the upper right and lower left of S account for periodicity in the circumferential direction. The product involving $S\mathscr{F}_T$ serves to suppress jaggedness in plots of the solution vector $\mathscr{F}_T$. The solution is expected to be discontinuous, so care is taken to assure that α_2 is as small as possible while still leaving the optimization robust.
- $\hat{H}_i$ employs the forward solution to map from applied tape loads to surface strain of type i around the circumference at cross section z_i. In the problem to be considered below, there are two strain gauge orientations, axial and circumferential, and two cross-sections on which the gauges are mounted, one on the male component and one on the female component. Thus i runs from 1 to 4. The term in Eq. (5.11) involving $S\hat{H}_i\mathscr{F}_T$ serves to suppress jaggedness in plots of the strains associated with solution vector $\mathscr{F}_T$. The correct solution is expected to be reasonably smooth, so this term should not degrade the quality of our answer.

The terms on the right hand side of Eq. (5.8) are, in order:

(a) the square error in matching experimental strains,

(b) a term proportional to the square of the force vector,

(c) a term roughly proportional to the square of the curvature of the force as measured around the circumference of the tape, and

(d) a term roughly proportional to the square of the curvature of each strain component as measured around the circumference of the tape.

Values of α_m are each chosen to be large enough to make the optimization process robust, but small enough so that when the minimization solution to J_1 of Eq. (5.11) is calculated using slightly different $\{\alpha_m\}$ and that solution is used to evaluate J_0 the result is reasonably independent of the $\{\alpha_m\}$.

An Exploitation of Axial Symmetry

In general, the matrix H is obtained by preforming a separate finite element calculation for each applied force $\{F_T(\theta_k)\}$. In the tape joint problem, the computational effort can be reduced by assuming axial symmetry. Of course exploiting axial symmetry calls for use of cylindrical coordinates where locations are identified by (r,ϕ,z). Let the strain at location (r,ϕ,z) due to a single pair of opposing element faces at θ_k be denoted as $\varepsilon(r,\phi,z,\theta_k)$. By superposition

$$\varepsilon(r,\phi,z) = \sum_k \varepsilon(r,\phi,z,\theta_k)\, F_T(\theta_k)\, r_T\, d\theta_k \tag{5.13}$$

Simplification derives from a Galilean transform

$$\varepsilon(r,\phi,z,\theta_k) = \varepsilon(r,\phi-\psi,z,\theta_k-\psi) \tag{5.14}$$

for all ψ. In particular, it applies for $\psi = \theta_k$

$$\varepsilon(r,\phi,z,\theta_k) = \varepsilon(r,\phi-\theta_k,z,\theta=0) \tag{5.15}$$

A single finite element calculation is performed with a force applied to a single pair of opposing element faces at $\theta = 0$. The full compliance matrix H can be constructed by a superposition of those results, providing matrix H of Eq. (5.7).

Chapter 6

The Quasi-Static Experiment

Test Specimen

The assembly experiments discussed below were performed on the same specimen as was used for the vibration experiments discussed in Chapter 2. (Refer to Figure 2.1 of that chapter.)

A close-up of the assembly in the vicinity of an insertion window and a close-up of the the female specimen alone in the vicinity of an insertion window are shown in Figure 6.1.

Figure 6.1: *The insertion window as seen in the assembled system and in the female component alone.*

The tapes in their original state and as they appear after having been used in a tape joint assembly and then removed are shown in Figure 6.2.

Strain Gauges

Axially and circumferentially oriented strain gauges are placed on the male and female components near the inter-component seam. Circumferential placement of the gauges is identified by angular distance from an origin centered at the window shown in Figure 6.1. A summary of gauge orientations and angular locations is presented in Table 6.1.

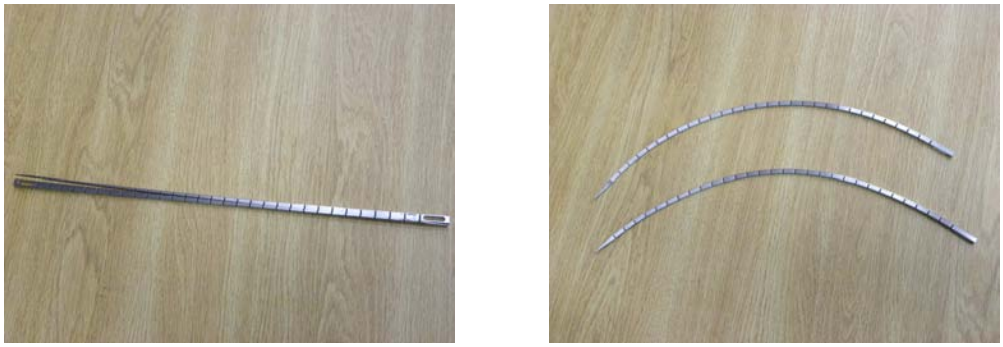

Figure 6.2: *The tapes in their original state and as they appear after having been used in a tape joint assembly and then removed.*

Angular Location	0°	15°	45°	90°	135°	150°	270°
Male Axial	X	X	X	X	X	X	X
Male Circum.	X	X	X		X	X	
Female Axial				X			X
Female Circum.				X			X

Table 6.1: Angular locations of strain gauges

The Test

The test consisted of the following steps

1. Suspend the female component so that its tape assembly section faces down.
2. Lift the male component up from below until it mates with the female section.
3. Zero all strain gauges.
4. Start recording of strain gauge channels.
5. Insert tapes, hammering them in as necessary.
6. Hammer on sides of assembled structure to permit tapes to settle.
7. Discontinue recording strain gauge signals.
8. Disassemble.

The above procedure was performed twice. We refer to data collected from the first and second assembly process as associated with Assembly 1 and Assembly 2, respectively. The steps in the test process are indicated in the annotations shown in Figure 6.3.

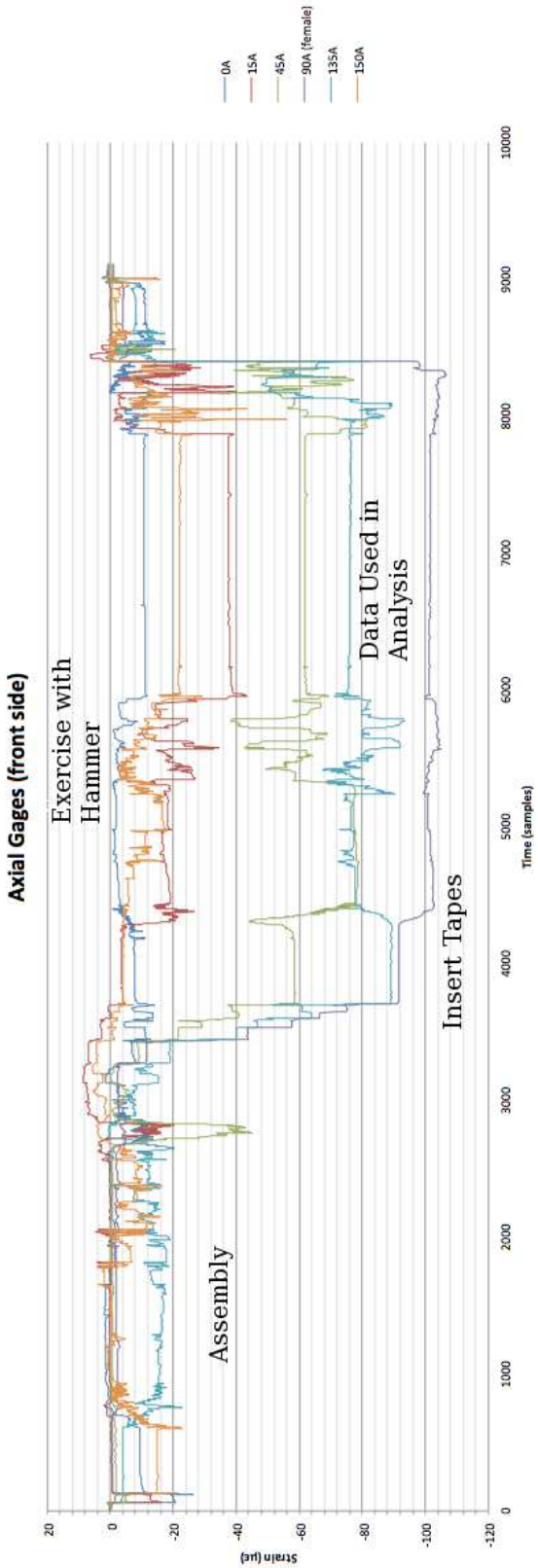

Figure 6.3: *The various steps in the testing process are reflected in the axial strain histories. These strains are from Assembly 1.*

In Figure 6.3 it is noted that the magnitude of the axial strain at 90° on the female component is substantially larger than the strains shown from the male component. This is made more obvious in Figure 6.4 where the strain is observed in the female component at 90° with those from the male component at that angle; the ratio is almost 2/1. Circumferential (hoop) strains are shown in Figure 6.5. There the hoop strains are seen to be substantially lower than the corresponding axial strains. This is not a surprise, since they are due primarily to Poisson effects. Strain data from the second assembly process are very similar to that shown from the first. (See Figures 6.6, 6.7, and 6.8.)

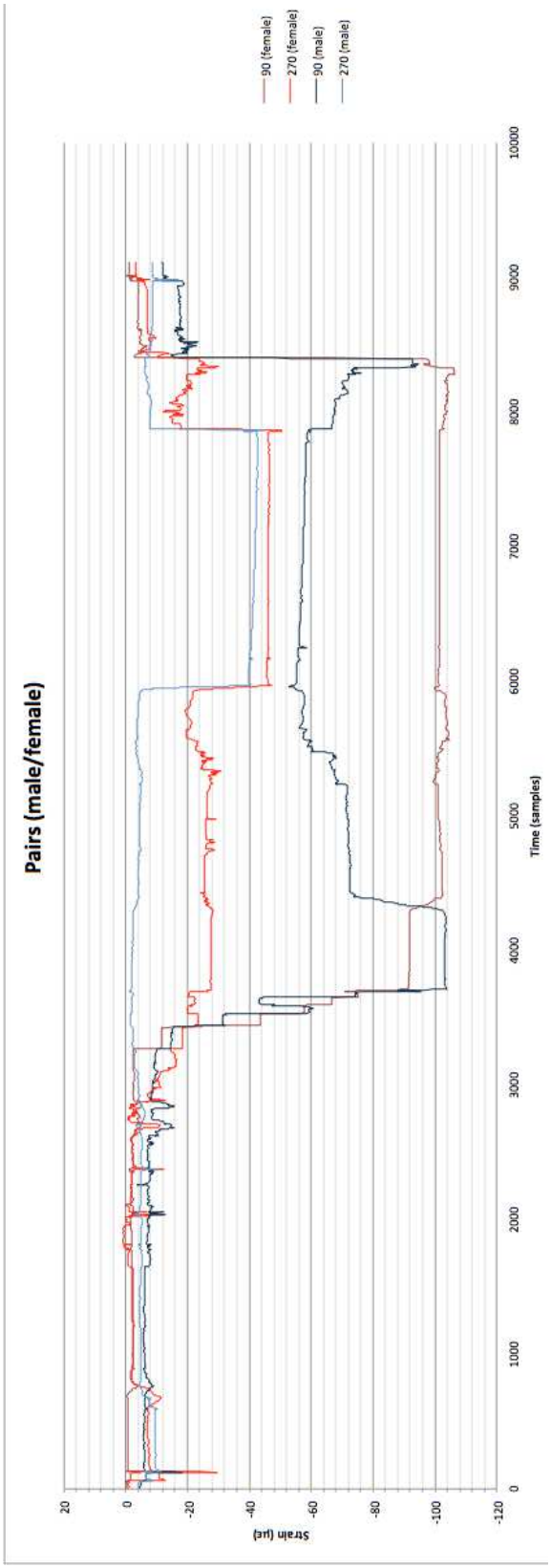

Figure 6.4: *Axial strains on the male and female components at* 90° *and* 270° *on Assembly 1.*

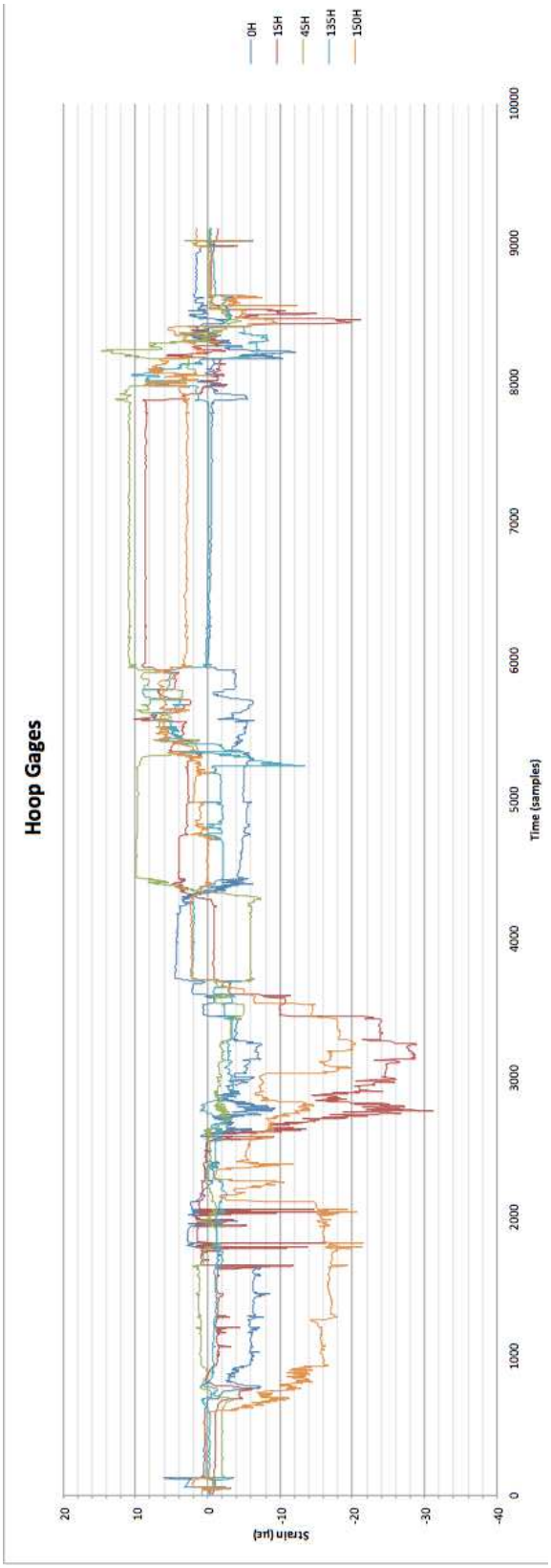

Figure 6.5: *Hoop strains from Assembly 1.*

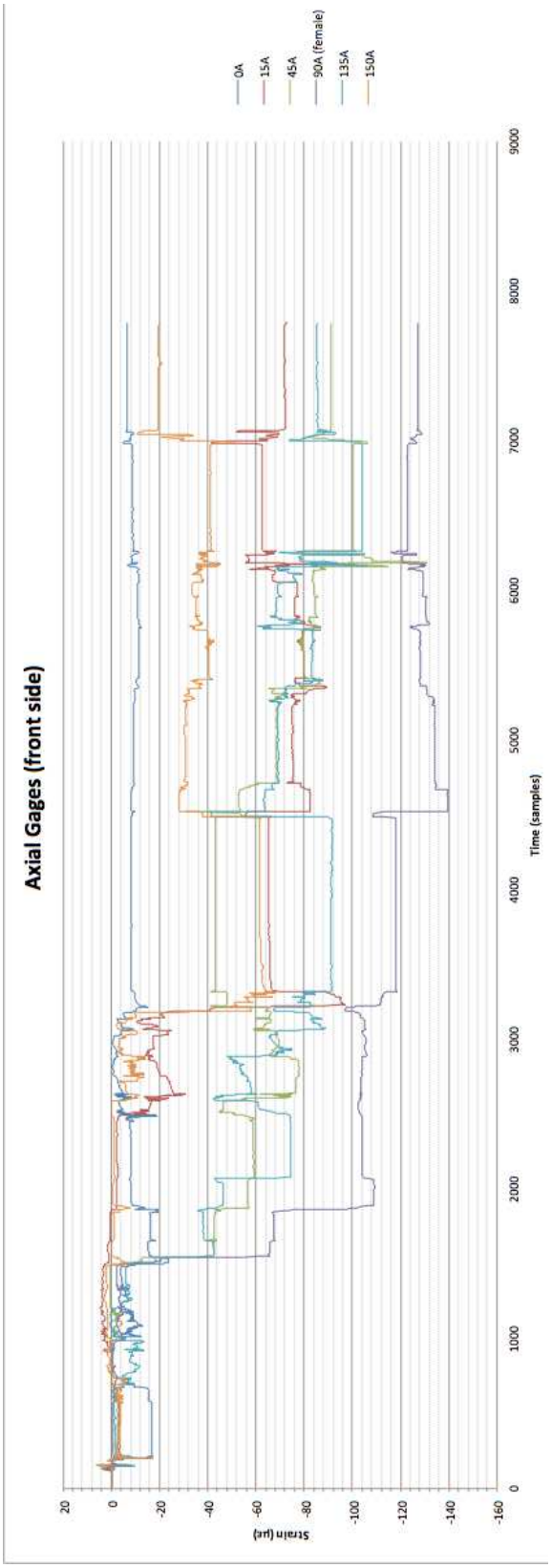

Figure 6.6: *Axial strain histories from Assembly 2.*

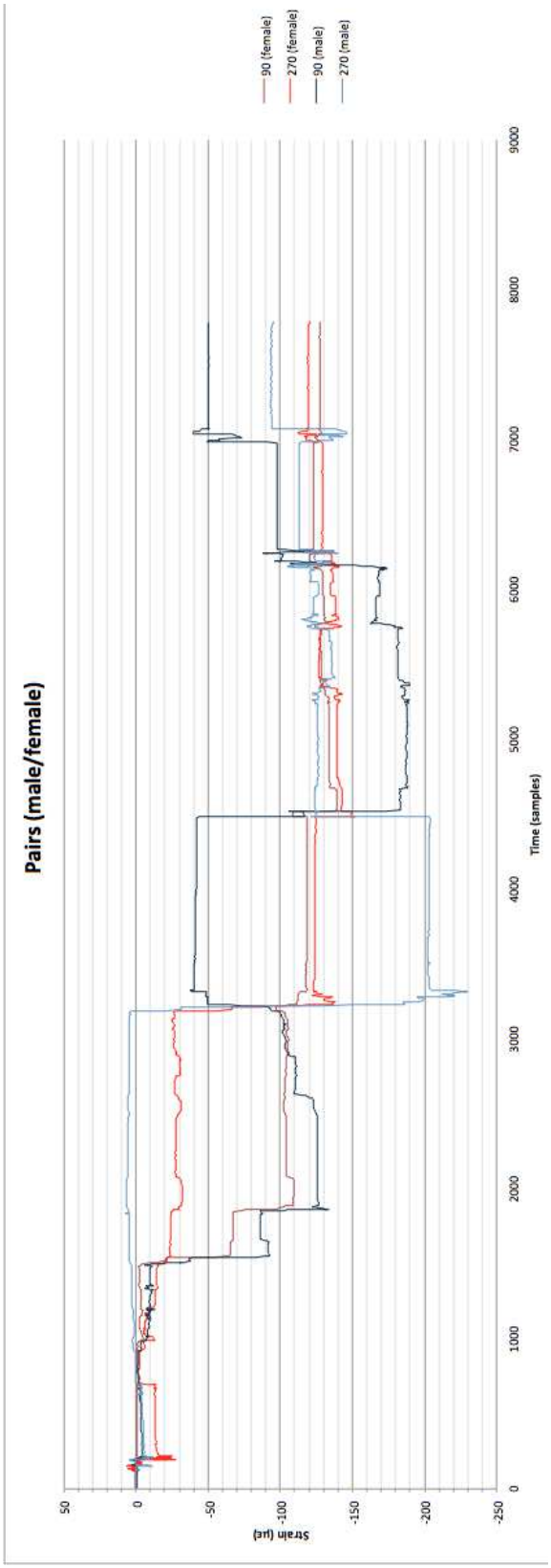

Figure 6.7: *Axial strains on the male and female components at* 90° *and* 270°.

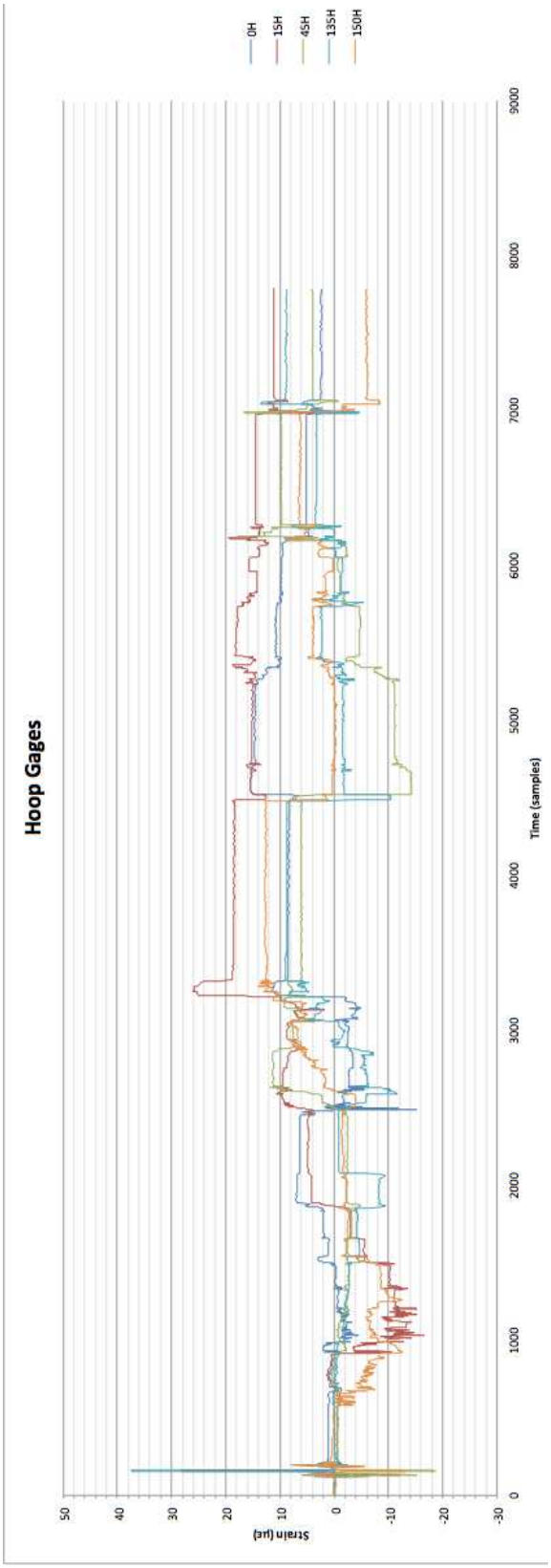

Figure 6.8: *Hoop strains from Assembly 2.*

Chapter 7

Finite Element Analysis

The single three-dimensional finite element analysis involving 106,000 elements was performed involving one set of loads on elements in the tape channel located approximately at zero degrees. A cross-sectional view of the the mesh containing the tape region is shown in Figure 7.1.

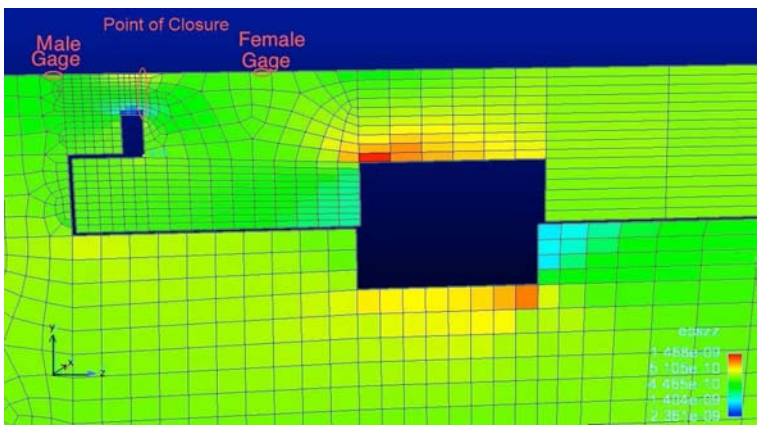

Figure 7.1: *Finite element mesh in vicinity of tape joint.*

As discussed near the end of Chapter 5, the elasticity of the system can be captured sufficiently by performing one finite element analysis, where equal and opposite concentrated forces are applied to the male and female portions of the tape track in the vicinity of $\theta = 0$. Axial symmetries permit the rest of elastic response to be captured through a sequence of angular transformations.

Axial strains of that single finite element analysis are shown in the mesh in Figure 7.1. Also indicated in that figure are the axial locations of the strain gauges on the male and female components. The circumferential distribution of surface strains on the male component due to a concentrated force at 0° are shown in Figure 7.2 and the corresponding strain distributions on the female component are shown in Figure 7.3.

The axial strains measured on the male body are expected to be generally much larger (by a factor of 5) than those on the female body according to a comparison of Figures 7.2 and 7.3. This would be consistent with the strain gauges on the female component being substantially further from the point of closure than are those on the male component. There is reason to be suspicious of the strains measured on the female components.

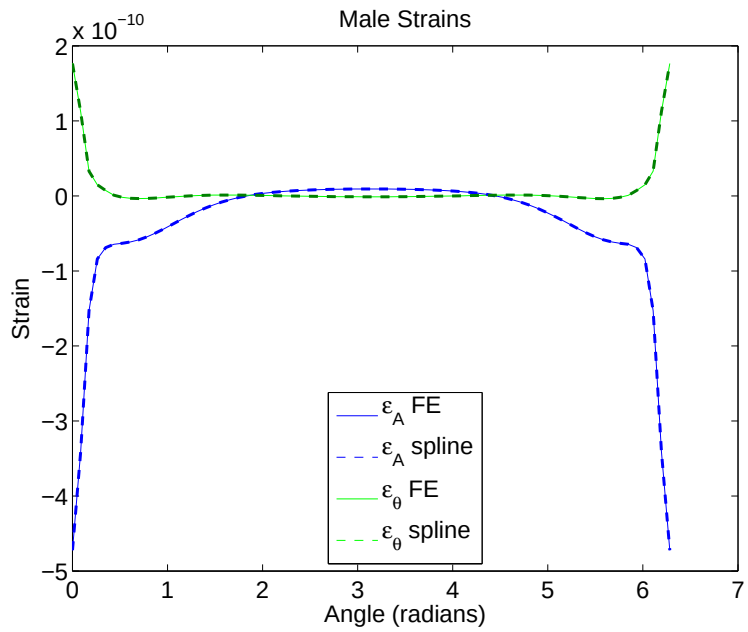

Figure 7.2: *Circumferential distribution of surface strains on the male component due to a concentrated force at* 0°.

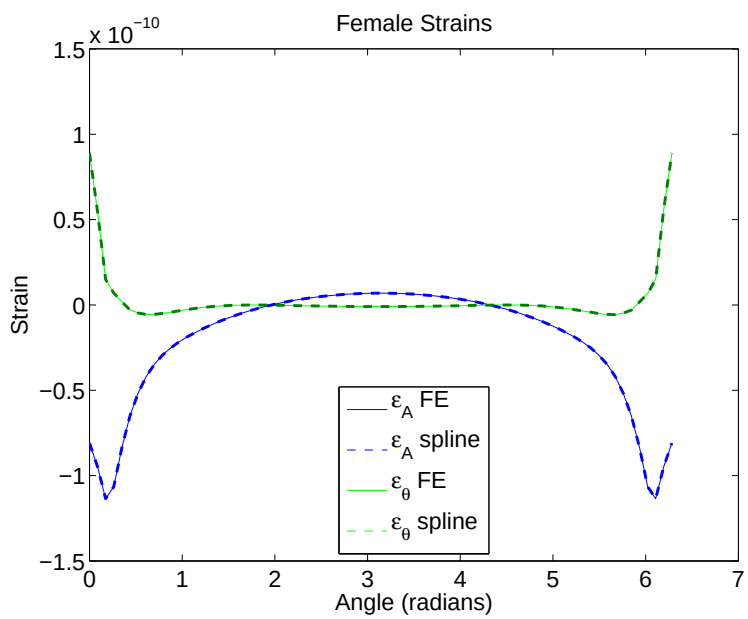

Figure 7.3: *Circumferential distribution of surface strains on the female component due to a concentrated force at* 0°.

Chapter 8

Results

It was impossible to match simultaneously strains measured on the female component and on the male component. Because the the female strains were suspicious already, it was decided to employ only the strains on the male component in the inverse problem for tape loads.

Assembly 1

The techniques discussed above employed the strain data collected on the male component of Assembly 1 to generate the tape load distribution (force/length) shown in Figure 8.1.

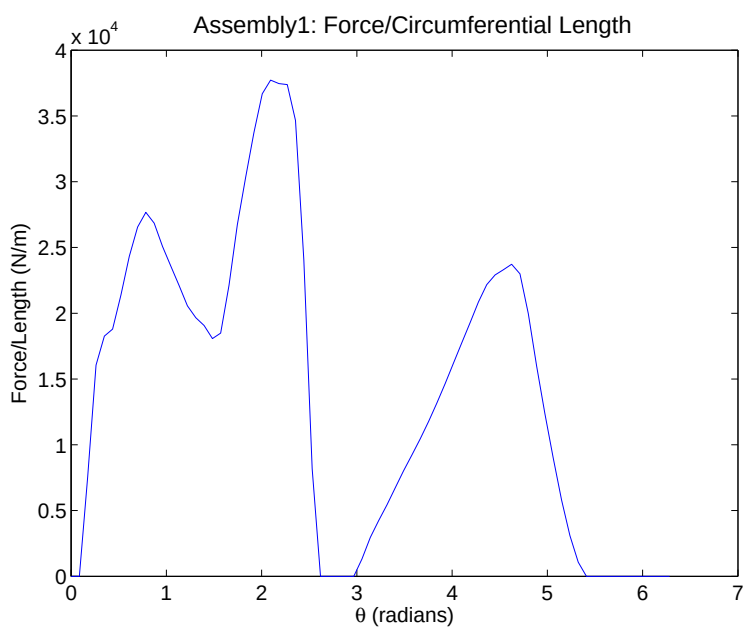

Figure 8.1: *Circumferential distribution of tape load computed for Assembly 1.*

How well the computed tape force distribution can reproduce the strains measured on the male component in Assembly 1 is indicated in Figures 8.2 and 8.3.

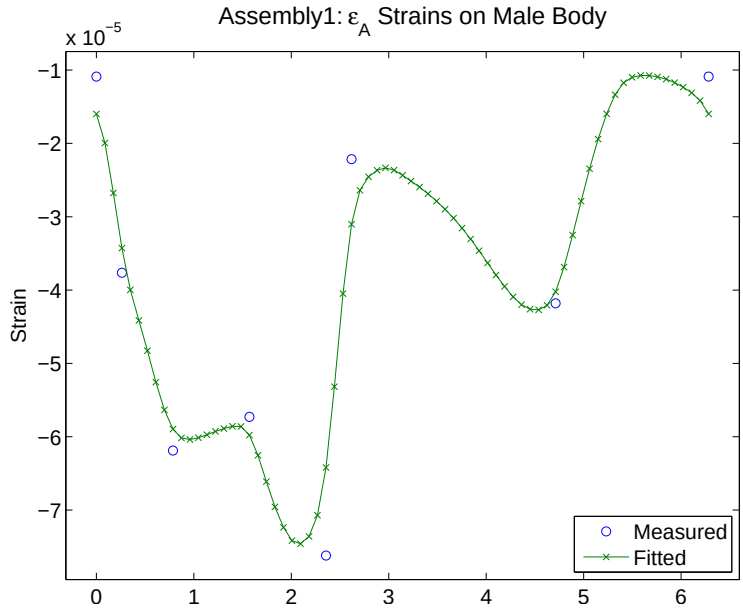

Figure 8.2: *Circumferential distribution of axial strain for Assembly 1 from measurement and from computed tape load.*

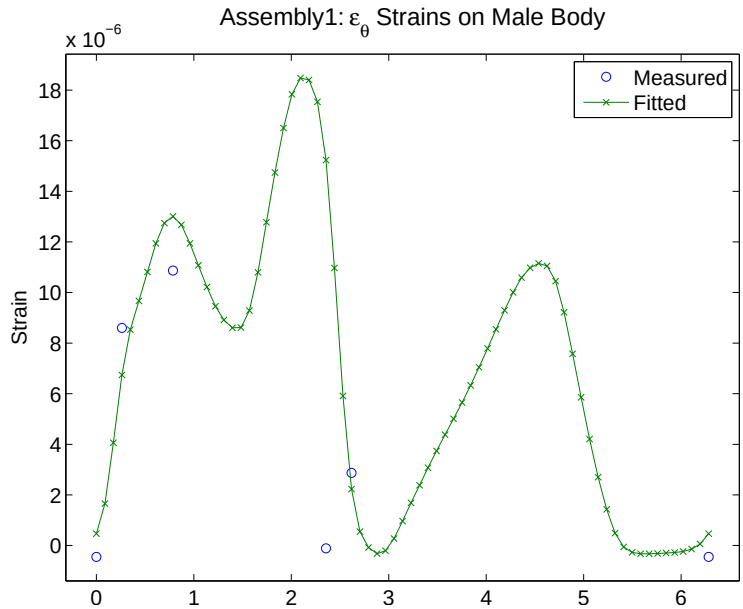

Figure 8.3: *Circumferential distribution of hoop strain for Assembly 1 from measurement and from computed tape load.*

Overall, it appears that the computed tape load distribution (Figure 8.1) can reproduce the measured strains on the male component in Assembly 1.

Assembly 2

The techniques discussed above employed the strain data collected on the male component of Assembly 2 to generate the tape load distribution (force/length) shown in Figure 8.4.

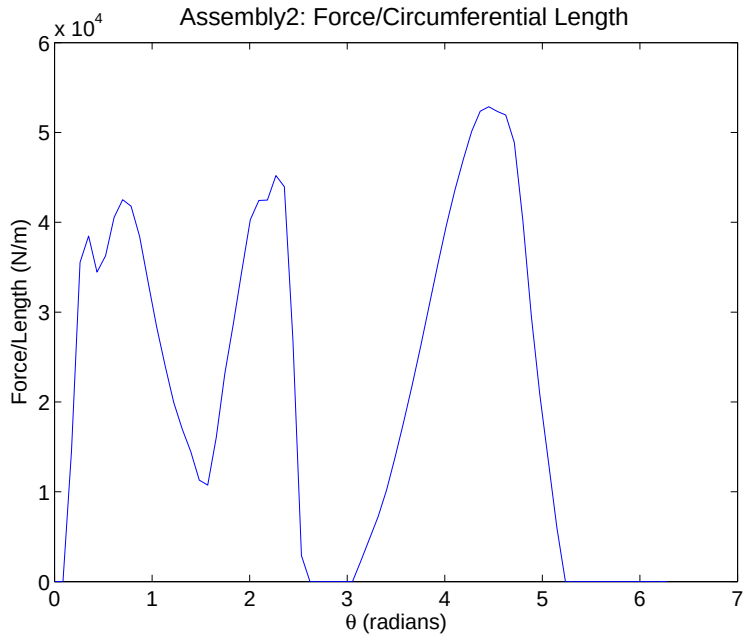

Figure 8.4: *Circumferential distribution of tape load computed for Assembly 2.*

How well the computed tape force distribution can reproduce the strains measured on the male component in Assembly 2 is indicated in Figures 8.5 and 8.6. Overall, it appears that the computed tape load distribution (Figure 8.4) can reproduce the measured strains on the male component in Assembly 2, but not as well as was the case for Assembly 1.

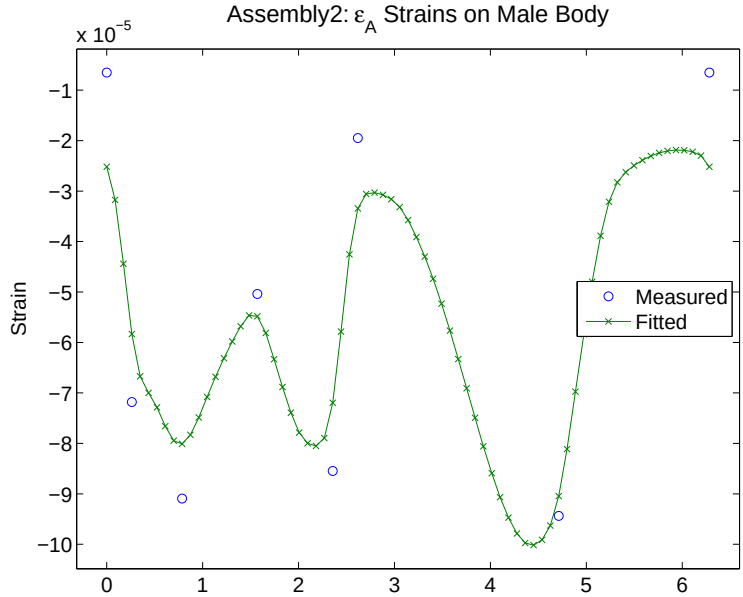

Figure 8.5: *Circumferential distribution of axial strain for Assembly 2 from measurement and from computed tape load.*

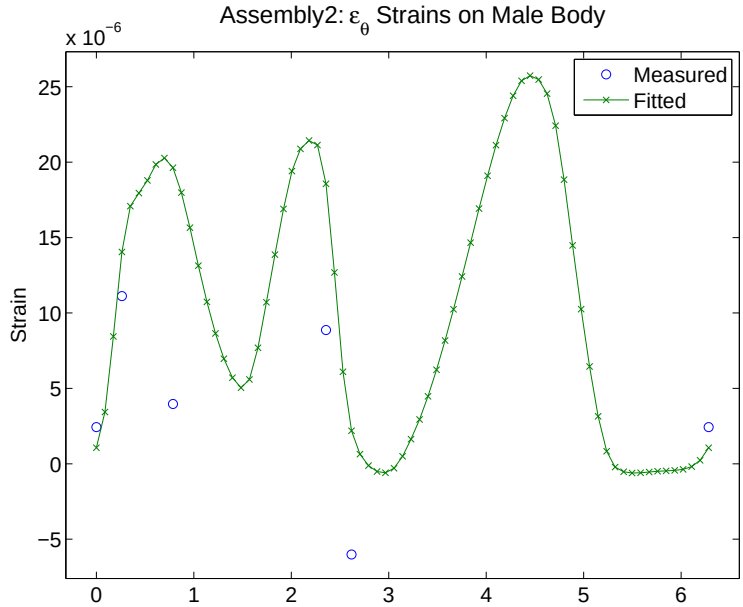

Figure 8.6: *Circumferential distribution of hoop strain for Assembly 2 from measurement and from computed tape load.*

Future Cautions

It is not too surprising that the strains measured on the female component were unreliable; correctly applying strain gauges is a notoriously difficult task. With that in mind, for future experimentation, it would be good to perform validation tests on the strain gauges before assembly of the full test structure.

An approach to such validation is the following:

1. Apply strain gauges at the desired locations on each of the male and female components.
2. Without attaching the components, apply known forces to the various locations on the "point of closure" on each component. Record the resulting strain gauge values.
3. Perform corresponding finite element analysis, evaluating strain at the locations of the gauges. This should be a well-conditioned analysis problem.
4. Confirm that the experimental strains and those obtained by finite element analysis agree.

Chapter 9

Conclusion

Several conclusions can be drawn from the work presented here:

- On the basis of the experiments reported here, tape-joined structures can be expected to be remarkably nonlinear in vibration that involves bending at the joint. This feature can be expected to have a major role in response of such structures when subject to lateral blast.
- Analytic predictions for dynamic response of tape-joined structures that do not account for this nonlinearity are going to be of very low fidelity.
- Understanding and ultimately predicting the joint nonlinearity requires some method of estimating the preloads in those joints. One method of doing so has been presented here. Yet more tools must be developed to use this information to understand and to predict quantitatively the structural nonlinearity of the joints.

Some candidate means of incorporating nonlinear dynamics of tape-jointed structures are: very low-order models (such as a Duffing equation) and techniques which incorporate the nonlinearity into integrated finite element analysis without solving contact problems at every time step. An approach for the latter is suggested in Appendix B.

References

[1] R. L. Alvis, “Mechanical considerations and design skills,” Sandia National Laboratories, Albuquerque, New Mexico, Sandia Report SAND2008-1124, March 2008, unlimited Release.

[2] R. P. Rechard, J. T. Black Jr., and S. D. Meyer, “Tape joint design guidelines,” Sandia National Laboratories, Albuquerque NM 87185, Sandia Report SAND83-1506, September 1983, unlimited Release Category UC-38.

[3] M. Huerta and J. T. Black, “Experimental and analytical investigation of an interlocking tape joint,” Sandia National Laboratories, Albuquerque, New Mexico, Sandia Report SAND76-0l66, March 1976, Unlimited Release.

[4] R. L. Alvis, “Joint utilizing wedgeshaped rectangular locking shafts,” U.S. Patent US 3 600 011, 08 17, 1971. [Online]. Available: http://www.google.com/patents/US3600011

[5] R. P. Rechard, “Tape joint stiffness,” Sandia National Laboratories, Albuquerque, New Mexico 87185, Sandia Report SAND86-0022, April 1986.

[6] T. Kalmár-Nagy and B. Balachandran, *The Duffing Equation: Nonlinear Oscillators and their Behaviour*. John Wiley and Sons, Ltd., 2011, ch. Forced harmonic vibration of a Duffing oscillator with linear viscous damping, pp. 139–174.

[7] M. N. Hamdan and T. D. Burton, “On the steady state response and stability of non-linear oscillators using harmonic balance,” *Journal of Sound and Vibration*, vol. 166, no. 2, pp. 255–266, 1993.

[8] P. R. Nayak, “Contact vibrations,” *Journal of Sound and Vibration*, vol. 22, no. 3, pp. 297–322, 1972, bolt Beranek and Newman Inc. Cambridge, Massachusetts 02138, U.S.A.

[9] M. D. Bryant, “Non-linear forced oscillation of a beam coupled to an actuator via Hertzian contact,” *Journal of Sound and Vibration*, vol. 99, no. 3, pp. 403–414, 1985, department of Mechanical and Aerospace Engineering, North Carolina State University, Raleigh, North Carolina 27695, U.S.A.

[10] J. Turner, “Non-linear vibrations of a beam with cantilever-Hertzian contact boundary conditions,” *Journal of Sound and Vibration*, vol. 275, p. 177191, 2004, e-mail address: jaturner@unl.edu (J.A. Turner).

[11] R. P. Rechard and R. L. Mayes, “Tape joint design for a vibration table,” Sandia National Laboratories, Albuquerque, NM, Sandia Report SAND84-1159, July 1984.

[12] G. H. Golub, P. C. Hansen, and D. P. O’Leary, “Tikhonov regularization and total least squares,” *SIAM Journal on Matrix Analysis and Applications*, vol. 21, no. 1, pp. 185–194, 1999. [Online]. Available: http://link.aip.org/link/SJMAEL/v21/i1/p185/s1&Agg=doi

[13] F. Ehrich and H. N. Abramson, “Nonlinear vibration,” in *Harris Shock And Vibration Handbook*, 5th ed., C. M. Harris and A. G. Piersol, Eds. McGraw-Hill, 2002, ch. 4, pp. 4.1–4.45.

[14] M. Brennan, I. Kovacic, A. Carrella, and T. Waters, “On the jump-up and jump-down frequencies of the duffing oscillator,” *Journal of Sound and Vibration*, vol. 318, no. 4-5, pp. 1250–1261, December 2008. [Online]. Available: http://eprints.soton.ac.uk/65213/

[15] A. H. Nayfeh and D. T. Mook, *Nonlinear Oscillations*, ser. Pure & Applied Mathematics Series. New York: John Wiley & Sons, 1979.

Appendix A

The Softening Duffing Oscillator

Duffing oscillators are simple harmonic oscillator devices containing a cubic restoring force. Such systems are well-studied and discussed lucidly in [13] and in [14]. They are often considered paradigms for nonlinear vibration.

In dimensionless form the governing equation for the forced Duffing oscillator subject to harmonic excitation is

$$y'' + 2\zeta y' + y + \alpha y^3 = cos\Omega\tau \tag{A.1}$$

If the coefficient α of that cubic term is positive, the system stiffens with amplitude. If the coefficient is negative, the system softens with amplitude.

This problem can be solved numerically by integrating over each period with the constraints that $y(0) = y(T)$ and $y'(0) = y'(T)$ where $T = 1/\Omega$. More often, such equations are addressed through the method of harmonic balance, where harmonics of the driving frequency and the Galerkin technique is employed to find the complex coefficient of each harmonic [15]. Consider just the first harmonic with

$$y(\tau) = \mathscr{R}\left(Y(\Omega)e^{i\Omega\tau}\right) \tag{A.2}$$

Substitution of Eq. (A.2) into Eq. (A.1) yields a cubic equation for $Y(\Omega)^2$ at each Ω. A feature of cubic equations with real coefficients is that there are always either one or three real solutions, so at each value of Ω there are always either one or three real solutions for Y^2 corresponding to one or three realizable solutions for $|Y(\Omega)|$. It is conventional to plot $|Y(\Omega)|$ vs Ω^2, and for negative α the locus of such solutions has the form of the black curve of Figure A.1.

At values of Ω^2 for which there are three solutions for $Y(\Omega)$, one of these is always unstable and not realized in steady state. The other two are quasi-stable and solutions may jump from one branch to another. On which branch a solution will be found depends on history, for instance:

- Sweeping through frequencies, starting at *low* Ω^2, where only one frequency exists (point A in the figure), the system amplitude tends to stay on the *lower* branch of the three-solution

regime until another one-solution regime is encountered. At that point the solution must "jump up" to that branch. This is a jump from point C to point D in the figure.

- Sweeping through frequencies, starting at *high* Ω^2, where only one frequency exists (point B in the figure), the system amplitude tends to stay on the *upper* branch of the three-solution regime until another one-solution regime is encountered. At that point the solution must "jump down" to that branch. This is a jump from point E to point F in the figure.

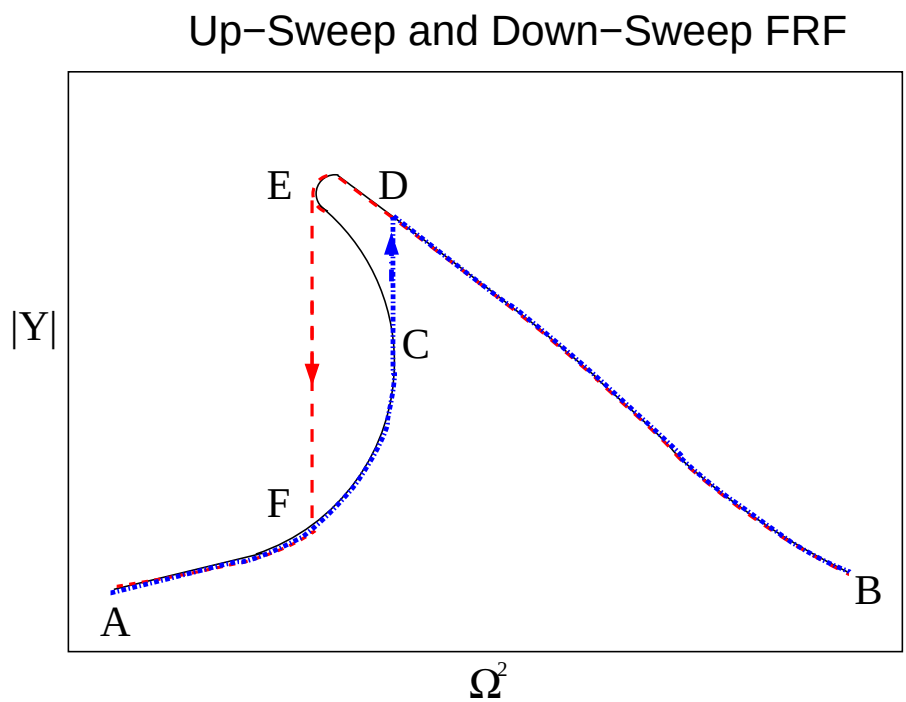

Figure A.1: *The softening Duffing oscillator admits multiple response amplitudes at fixed amplitude of harmonic excitation. "Up-jumps" and "down-jumps" in amplitude occur at the driving frequency is swept up or down, respectively.*

Several observations should be made about the *up-jump* and *down-jump* processes:

1. The *up-jumps* accompanying up-sweeps in frequency occur at frequencies higher than the frequencies associated with *down-jumps* accompanying down-sweeps in frequency.
2. The peak displacement amplitudes associated with the em up-jumps is *lower* than the peak displacement amplitudes associated with the *down-jumps*.
3. The jump displacement *always* occurs on the left side of the peak; the peak has infinite slope on the left and more gradual fall-off on the right.

Appendix B

A Reduced Tape-Joint Model for Finite Element Analysis

Solution of contact is computationally intensive. Retaining the nonlinear, but nearly elastic contribution of the tape joint to the dynamics of an assembled structure in a computationally tractable manner requires some substitute for solving the contact problem at every time step. Far better would be implementation of some method capturing the nonlinearity in a manner consistent with finite element model formulation, but providing explicit force-type output as a function of kinematic quantities.

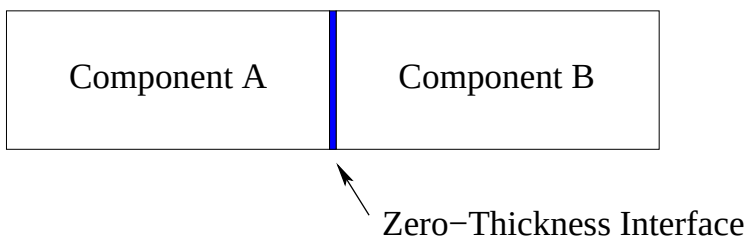

Figure B.1: *The assembled system is modeled as two physical components jointed by a zero-thickness interface whose properties are to be found.*

Consider the system shown in Figure B.1. The system consists of two physical components connected by a nonlinear zero-thickness interface. The properties of the interface are determined by comparison with a reference system consisting of the two physical components above, but as though the components were welded together.

Consider a bending oscillation as suggested by Figure 3.1. Either via detailed nonlinear finite element analysis accounting for contact or from experiment, one may deduce the compliance that the interface introduces to the system. For instance, for the case of low amplitude oscillation, the difference between measured natural bending frequency and that which would be calculated for the reference system can be ascribed to the presence of the interface. In the regime of very low amplitude oscillations, that compliance would be a constant number. At higher amplitudes of vibration, a nonlinear interface elasticity, $M(\phi)$, might be deduced. Here M is the effective moment applied over the interface cross section and ϕ is the finite rotation associated with that moment.

The unknown interface model must be constructed so as to reproduce $M(\phi)$. To do this, an

infinitesimally thick layer of material (film) that is capable of finite stretch in the normal direction is considered (Figure B.2). The deformation of that layer is treated as a monotonically increasing functions of normal traction.

The constitutive equation for the film is of the form

$$\sigma = f(u) \tag{B.1}$$

where σ is the normal traction and u is the corresponding finite displacement.

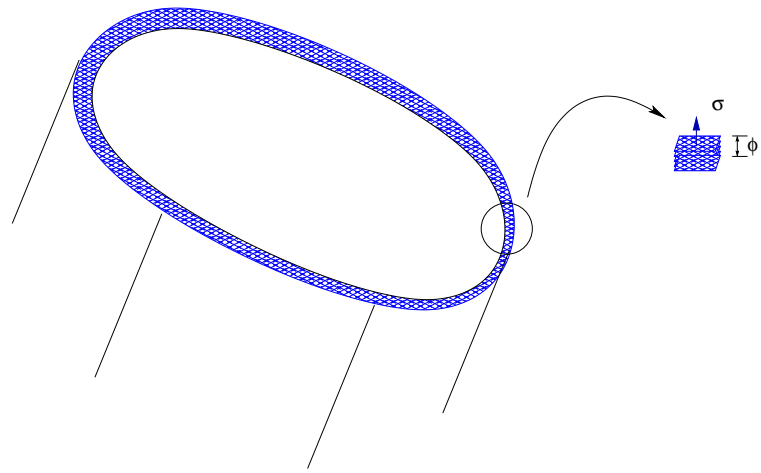

Figure B.2: *The joint is modeled as a finitely deformable, but infinitesimally thick material.*

It is necessary to make some kinematic assumptions connecting the local deformation of the interface layer with the overall relative rotation of the left and right components. This is accomplished by making the usual beam-bending assumptions:

1. Plane surfaces remain plane.
2. Stretch is proportional to distance from the neutral axis.
3. The neutral axis is on the centroid of the cross section.

These assumptions are somewhat redundant with each other, but their enumeration is helpful.

The kinematic assumptions above are expressed mathematically by

$$u = \phi y \tag{B.2}$$

where u is the stretch of the interface material a distance y from the neutral axis.

The moment is

$$M(\phi) = \int_A y f(u(y)) dA = \int_A y f(\phi y) dA$$

$$= \int_y y f(\phi y) w(y) dy \tag{B.3}$$

where $w(y)dy = dA$.

The above has the character of a Volterra integral equation of the first kind and can be solved by any of several standard methods.

Implementation in a finite element code should be fairly straight-forward. Zero thickness elements are defined in the interface. Topology of the elements will be that of a squashed hex element. The material properties are uniform among the elements in a particular interface and can be specified in the usual manner. Though these elements are nonlinear, they are elastic so their implementation should not be substantially more difficult than that of the more common bi-linear elements.

If there is asymmetry in the bending response, for example, bending vibration at small amplitude occurs in two orthogonal planes and at different natural frequencies, then the development can proceed as follows:

1. Postulate the existence of two species of nonlinear interface material, say type A and type B.
2. Postulate the distribution of the type A to go as $\sin\theta$ where $\theta = 0$ is on the neutral axis of the first bending mode.
3. Postulate the distribution of the type B to go as $\cos\theta$.
4. Generate and solve two coupled linear integral equations to capture the two bending responses $M_A(\theta)$ and $M_B(\theta)$.

DISTRIBUTION:

1 Professor Lawrence Bergman
306 Talbot Lab
104 S. Wright St.
University of Illinois
Urbana, IL 61801

1 Daniel Badders
LLNL
P.O. Box 808, L-125
Livermore, CA 94550

1 Miles A. Buechler
Los Alamos National Laboratory, W-13
P.O. Box 1663, MS T080
Los Alamos NM USA, 87545

1 Melih Eriten
Department of Mechanical Engineering
University of Wisconsin, Madison
Mechanical Engineering Building
1513 University Avenue
Madison, WI 53706-1572

1 Robert Ferencz
LLNL
P.O. Box 808, L-125
Livermore, CA 94550

1 Professor Dane Quinn
Dept. of Mechanical Engineering
The University of Akron
Akron, OH 44325-3903

1 Professor Alexander Vakakis
3003 Mechanical Engineering Laboratory
1206 West Green Street, MC-244
Urbana, IL 61801

1	MS 0346	Clark R. Dohrmann, 01542
1	MS 0346	D. Gregory Tipton, 01523
1	MS 0346	Diane E. Peebles, 01526
1	MS 0346	Michael A. Guthrie, 01523
1	MS 0346	Michael J. Starr, 01526
1	MS 0346	Michael Ross, 01523

1	MS	0346	Mikhail Mesh, 01523
1	MS	0346	Richard V. Field, 01526
1	MS	0346	Wil A. Holzmann, 01523
1	MS	0372	Chi S. Lo, 01524
1	MS	0372	Kenneth W. Gwinn, 01524
1	MS	0380	Garth M. Reese, 01542
1	MS	0380	Joseph Jung, 01542
1	MS	0386	Timothy S. Edwards, 01527
1	MS	0431	John Pott, 00511
1	MS	0557	Brandon Zwink, 01522
1	MS	0557	Darrick M. Jones, 01521
1	MS	0557	David Epp, 01522
1	MS	0557	Eric C. Stasiunas, 01521
1	MS	0557	Fernando Bitsie, 01521
1	MS	0557	Jerry W. Rouse, 01523
1	MS	0557	Laura Jacobs-O'Malley, 01521
1	MS	0557	Randall L. Mayes, 01522
1	MS	0557	Todd W. Simmermacher, 01523
1	MS	0828	Walter R. Witkowski, 01544
1	MS	0840	Justine E. Johannes, 01520
1	MS	0942	Wei-Yang Lu, 08256
1	MS	1070	Matthew R. Brake, 01526
1	MS	9013	James P. Lauffer, 08231
1	MS	9042	Michael D. Jew, 08259
1	MS	9042	Mike Chiesa, 08259
1	MS	9042	Mary E. Gonzales, 08250
5	MS	9042	Daniel J. Segalman, 08259
1	MS	0899	Technical Library, 9536 (electronic copy)

Sandia National Laboratories